Semnan University

Progress in Physics of Applied Materials

journal homepage: https://ppam.semnan.ac.ir/

Influence of Zinc Concentration and Sulfurization on the Physical Properties of CZTS Thin Films: Synthesis and Characterization

M.S. Sarmalek, M. Adelifard*

School of Physics, Damghan University, Damghan, Iran.

ARTICLE INFO

Article history:
Received: 12 December 2023
Revised: 26 December 2023
Accepted: 28 December 2023

Keywords:
Copper Zinc Tin Sulfur
Optical properties
Electrical properties
Sulfurization

ABSTRACT

This study focused on the synthesis and characterization of CZTS thin films using a spray pyrolysis method followed by sulfurization. Three different samples were prepared by varying the molar ratios of zinc to tin: Cu_2ZnSnS_4 (PV), $Cu_2Zn_{0.9}Sn_{1.1}S_4$ (NC), and $Cu_2Zn_{1.1}Sn_{0.9}S_4$ (PC). The samples were annealed in the presence of sulfur at 300°C X-ray diffraction (XRD) analysis revealed the formation of a kesterite crystal structure in all samples, with the (112) plane being the dominant orientation. The CZTS thin films showed a maximum crystallite size of 11.6 nm in the PC sample. Field emission scanning electron microscopy (FESEM) was used to investigate the morphological properties, providing insights into the surface characteristics and microstructure of the thin films. The optical properties of the CZTS thin films were examined using UV-Vis spectroscopy. It was observed that the band gap energy increased in all samples after sulfurization, ranging from 1.50 eV to 1.66 eV. This indicates the potential suitability of the films as absorber layers in solar cell applications. The electrical properties were evaluated through Hall effect measurements, which revealed that the CZTS thin films exhibited p-type conductivity. The NC sample demonstrated the lowest specific resistivity of 1.43 Ω.cm.

1. Introduction

The investigation of light-absorbing layers that are free from rare and toxic elements is vital for the development of affordable and widely applicable solar cells [1]. Copper-based chalcopyrite materials have garnered significant attention as promising options for photoabsorbing layers in low-cost thin film solar cell applications [2]. Currently, CdTe and $Cu(InGa)Se_2$ (CIGS) technologies lead the solar cell industry and are commercially available. However, the toxicity of cadmium and the scarcity of tellurium limit the potential of CdTe-based solar cells. Similarly, CIGS thin films contain toxic selenium, and the use of gallium and indium, which are not abundant, presents further challenges [3].

In recent years, compounds featuring the kesterite crystalline structure have emerged as highly promising and abundant earth-abundant materials for thin film solar cell applications [4]. Among these compounds, Cu_2ZnSnS_4 (CZTS) stands out as a quaternary compound with a p-type carrier characteristic and a band gap ranging from 1.4 to 1.6 eV [5]. With its high absorption coefficient of 10^4 cm^{-1} and composition consisting of non-toxic elements, CZTS represents a compelling option for low-cost absorbent layers in thin solar cells [6]. According to the Schweizer-Quizzer Theory, CZTS has the potential to achieve an impressive energy conversion efficiency of 32.2% [7]. However, to date, practical efficiency levels have remained lower, with a vacuum-based approach achieving an efficiency of 9.3% [8].

CZTS compounds exist in two main crystalline structures known as kesterite and stannite, with orientations along the (112) and (220) planes [9]. Both structures have a tetragonal crystalline phase, and their structural differences are related to different sub-network cation guidelines [10]. To distinguish between these two neutron spectroscopy structures, specialized methods are required

* Corresponding author.
E-mail address: adelifard@du.ac.ir

Cite this article as:
Sarmalek, M.S. and Adelifard, M., 2023. Influence of Zinc Concentration and Sulfurization on the Physical Properties of CZTS Thin Films: Synthesis and Characterization. *Progress in Physics of Applied Materials*, *3*(2), pp. 185-194 DOI: 10.22075/PPAM.2023.32622.1077

[11]. There are various methods for depositing CZTS thin films, including RF magnetron sputtering deposition [12], thermal evaporation [13], pulsed laser deposition [14], spray pyrolysis deposition [15], sol-gel deposition [16], photochemical deposition [17], and aqueous bath deposition [18]. The spray pyrolysis method is a simple and cheap method. Morphology, electrical, and optical properties of CZTS thin films are adjustable by changing the Zn:Sn molar ratio and deposition parameters such as the amount sprayed, the distance between the nozzle and the sample, the speed of spraying the solution and Sulfurization. Nakayama and Ito [19] reported spray deposited CZTS thin films followed by annealing the films under 5 % H_2S gas flow. Kumar et al. [20] studied the effects of substrate temperature, starting solution pH, copper salt and thiourea concentrations on the growth and properties of spray deposited CZTS films. Kameyama et al reported structural, morphological, and compositional characterization of CZTS films [21].

In this study, we have focused on examining the impact of different zinc to tin molar ratios on the growth and characteristics of thin films made of copper zinc tin sulfide (CZTS). To achieve this objective, we employed an aqueous solution containing copper acetate, tin chloride, zinc acetate, and thiourea, and deposited the films at substrate temperatures of 325°C. Subsequently, sulfurization was carried out in a sulfur atmosphere. Throughout the research, we thoroughly investigated the samples from multiple perspectives, including their structural properties such as crystallinity and surface morphology. Additionally, we analyzed the optical properties by estimating the band-gap energy. Furthermore, we conducted electrical measurements to assess the resistivity and performed Hall effect measurements to gain insights into the electrical behavior of the samples. These comprehensive analyses allowed us to gain a comprehensive understanding of the CZTS thin films produced under different zinc to tin molar ratios.

2. Experimental

To obtain the stochiometric Cu_2ZnSnS_4 (CZTS) thin film, we used 0.04 M copper acetate, 0.02 M zinc acetate, 0.02 M tin chloride, and 0.08 M thiourea as copper, zinc, tin, and sulfur sources, respectively. To improve the solubility of tin chloride, a few drops of hydrochloric acid were also added to the 1000 ml of distilled water to give a Cu:Zn:Sn:S molar ratio of 2:1:1:4. The final CZTS solution was stirred for about 30 minutes and then sprayed onto the glass substrates at 325°C. The sample is denoted as 'PV'. In order to examine the impact of zinc content on the physical properties of the samples under investigation, the molar ratio of zinc to tin ([Zn]:[Sn]) in the base solution was varied. The samples with molar ratios of 2:0.9:1.1:4 ($Cu2Zn0.9Sn_{1.1}S_4$) and 2:1.1:0.9:4 ($Cu2Zn1.1Sn_{0.9}S_4$) were designated as 'NC' and 'PC' respectively. Subsequently, the annealing process was conducted in the presence of sulfur at a temperature of 300°C for a duration of 30 minutes under an argon gas atmosphere. The resulting films were labeled as 'PVs', 'NCs', and 'PCs'. Prior to annealing, the films exhibited a consistent thickness of 300 nm, as confirmed by cross-sectional FESEM imaging. Following annealing, the thickness increased to 500 nm. The production steps involved in creating the layers are illustrated in Figure 1.

The crystalline structure was analyzed by X-ray diffraction (XRD) spectrum using a D8 Advance Bruker system using Cu–Ka radiation (k = 1.5406Å). The optical characterization of the samples was performed by Shimadzu-UV1800 spectrophotometer in the spectral range of 400–1100 nm. The morphology and elemental composition were determined using field emission scanning electron microscopy model MIRA3. The electrical resistivity and Hall effect data (magnetic field strength =240 mT) of the samples were measured in the Van der Pauw configuration.

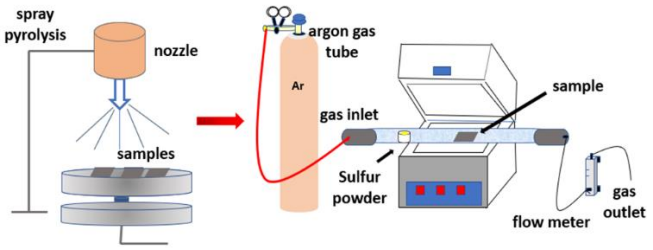

Fig. 1. Summary of the procedure for depositing CZTS films.

3. Results and discussion

3.1. XRD studies

Fig. 2 presents the X-ray diffraction (XRD) patterns of the investigated samples deposited at various Zn/Sn molar ratios. As depicted in Figure 2, a distinct diffraction peak at 28.53° is observed in all thin films, corresponding to the (112) preferred orientation plane of CZTS with a kesterite phase (JCPDS 00-026-0575) [22]. Furthermore, the PCs sample, following annealing, exhibits a diffraction peak at 47.33°, indicative of the (220) indices, which is consistent with previous findings. Notably, the intensity of the diffraction peaks in the annealed samples is enhanced in the presence of sulfur, indicating an improvement in crystal order. It is worth mentioning that no secondary phases associated with CuS or ZnS were detected in the XRD patterns of the samples before and after the sulfurization process, as reported in the literature [23].

Using Scherer's formula:

$$D = \frac{0.9\,\lambda}{\beta\,\cos\theta} \tag{1}$$

where D is the average crystallite size, λ is the wavelength of the X-rays, β is full width at half maximum of the main peak, k is a constant (close to unity) and θ is the Bragg angle. The calculated crystallite sizes are found to be 7.3, 6.3, 5.8, 8.6, 10.7, and 11.6 nm for PV, PVs, NC, NCs, PC, and PCs, respectively (Table 1). In the NC and PC samples, the size of the crystals increased after annealing and decreased in the PV sample. The variation of the crystallite size has major influence on optical and electrical properties of the samples. In poly-crystalline thin film semiconductors, increasing the dimensions of nanocrystals increases carrier mobility and also the decrease of crystallite size decreases the carrier mobility [24].

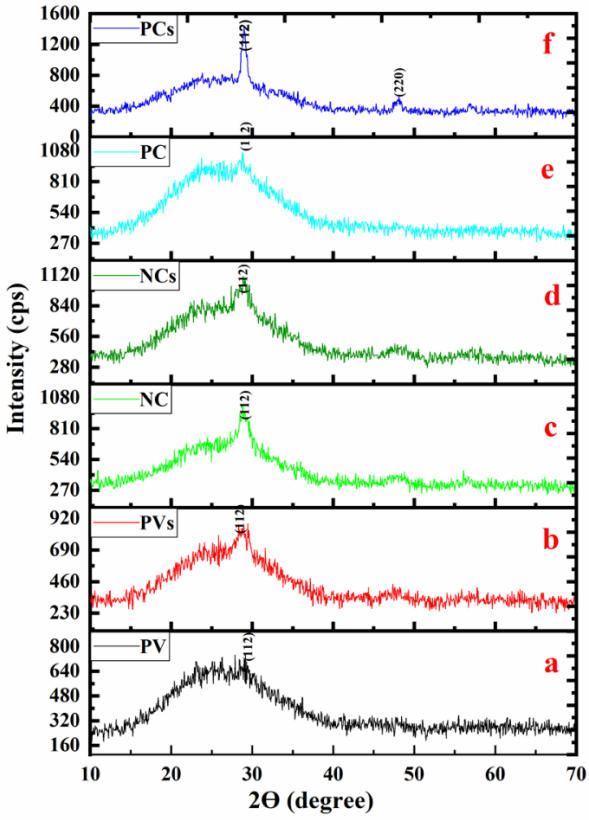

Fig. 2. XRD patterns of the studied samples before and after sulfurization process.

3.2. Morphological studies

According to Figure 3(a), the PV layer exhibits a relatively smooth surface with streaks. At lower magnification, the images reveal porous surfaces, and the accumulation of small-grained particles leads to cluster formation on the substrate surface. After annealing at 300°C, the smaller clusters merge, resulting in larger clusters and increased seed size (Figure 3(b)). The average grain dimensions of the PV layer increased from 27-32 nm before annealing to 32-53 nm after annealing. (Figure 3(c)). In Figure 4 (a), the smooth surface of the sample shows a noticeable accumulation of seeds, particularly at lower magnification. After annealing (Figure 4(b)), the formation of cluster structures becomes evident. The NC layer had average grain dimensions ranging from 45-59 nm before annealing, which decreased to 34-54 nm after annealing. Figures 5 (a) and (b) display images of the PC layer ($Cu_2Zn_{1.1}Sn_{0.9}S_4$) before and after annealing, respectively. Initially, the PC layer has a uniform surface with slight porosity. However, after annealing, there is a significant increase in the accumulation of seeds, leading to the formation of multidimensional structures. The PC layer exhibited an initial average grain size of 21-25 nm, which substantially increased to 66-125 nm after moderate annealing. Large grain sizes are desirable for achieving high-efficiency solar cells. Increasing the size of nanocrystals reduces the occurrence of grain boundaries, resulting in reduced recombination and increased effective diffusion length of minority carriers. These factors contribute to a higher short-circuit photocurrent in polycrystalline solar cells [25].

Table (2) provides information on the Elemental Energy Dispersive X-ray (EDX) analysis of PV, NC, and PC thin films before and after annealing in the presence of sulfur. The results show the ratio of sulfur element to the other metals is higher compared to the expected elemental composition. However, after annealing, the sulfur ratio decreases, except for the PC sample. This decrease in sulfur ratio suggests the possibility of sulfur evaporation from the sample surfaces during annealing. Furthermore, all the prepared layers, both before and after annealing, are found to be rich in copper and exhibit deficiencies in terms of the (Cu/(Zn + Sn>1)) and (Zn/Sn <1) ratios. Additionally, the Zn/Sn ratio increases in all samples after annealing.

Table 1. The average crystallite size for the CZTS thin films.

Sample	2Θ(deg)	D (nm)
PV	28.44	7.3
PVs	28.78	6.3
NC	28.9	5.8
NCs	28.93	8.6
PC	28.7	10.7
		11.6
PCs	29.92	

Table 2. Energy dispersive X-ray analysis (EDX) of the samples.

Sample	Zn/Sn	Cu/(Zn+Sn)	S/(Cu+Zn+Sn)
PV	1.11	1.24	1.21
PVs	1.16	1.25	0.88
NC	0.26	1.02	1.1
NCs	0.29	0.93	0.98
PC	0.39	1.09	1.07
PCs	0.4	1.18	1.21

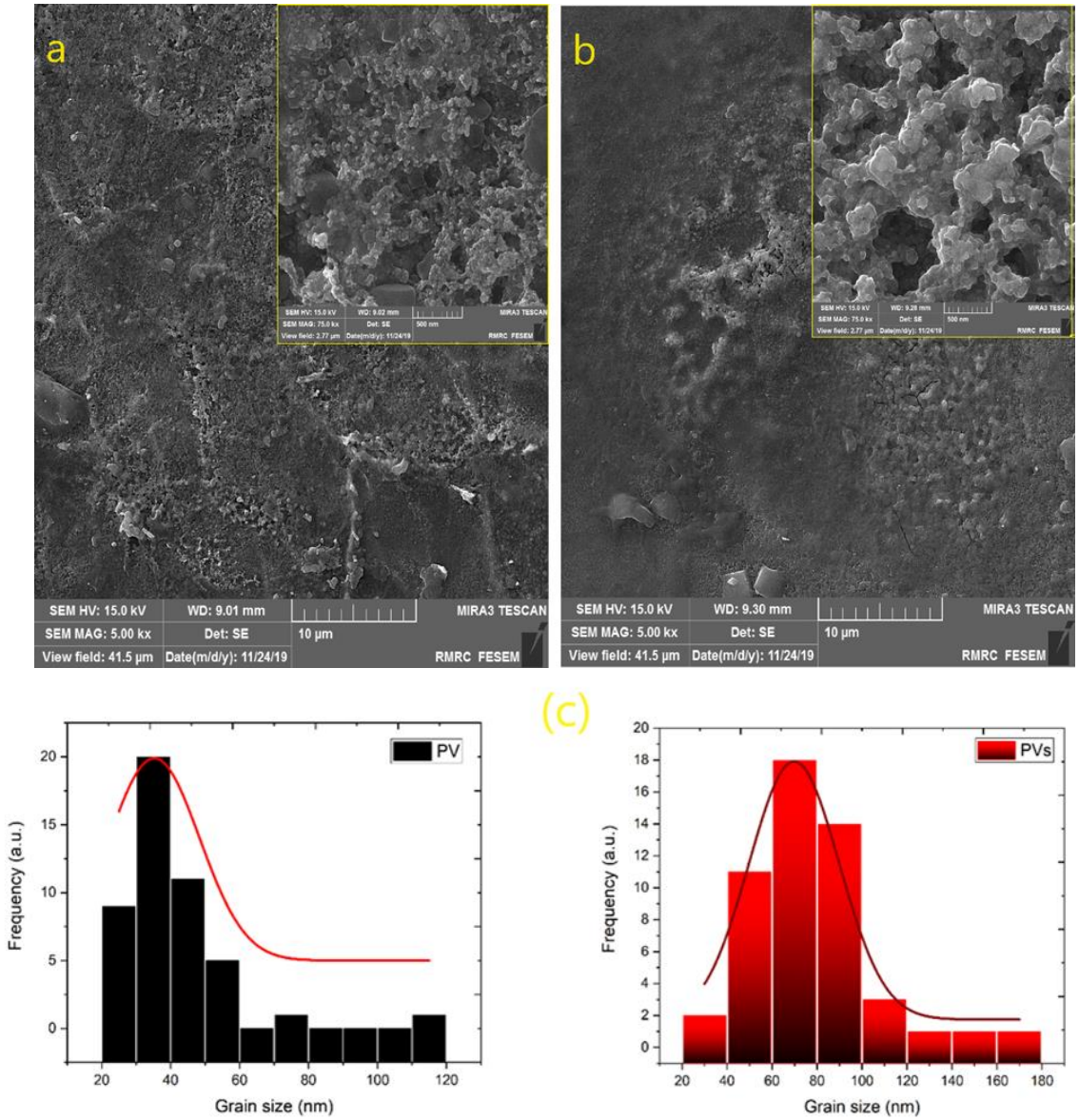

Fig. 3. FESEM images and grain size distribution of both PV and PVs thin films.

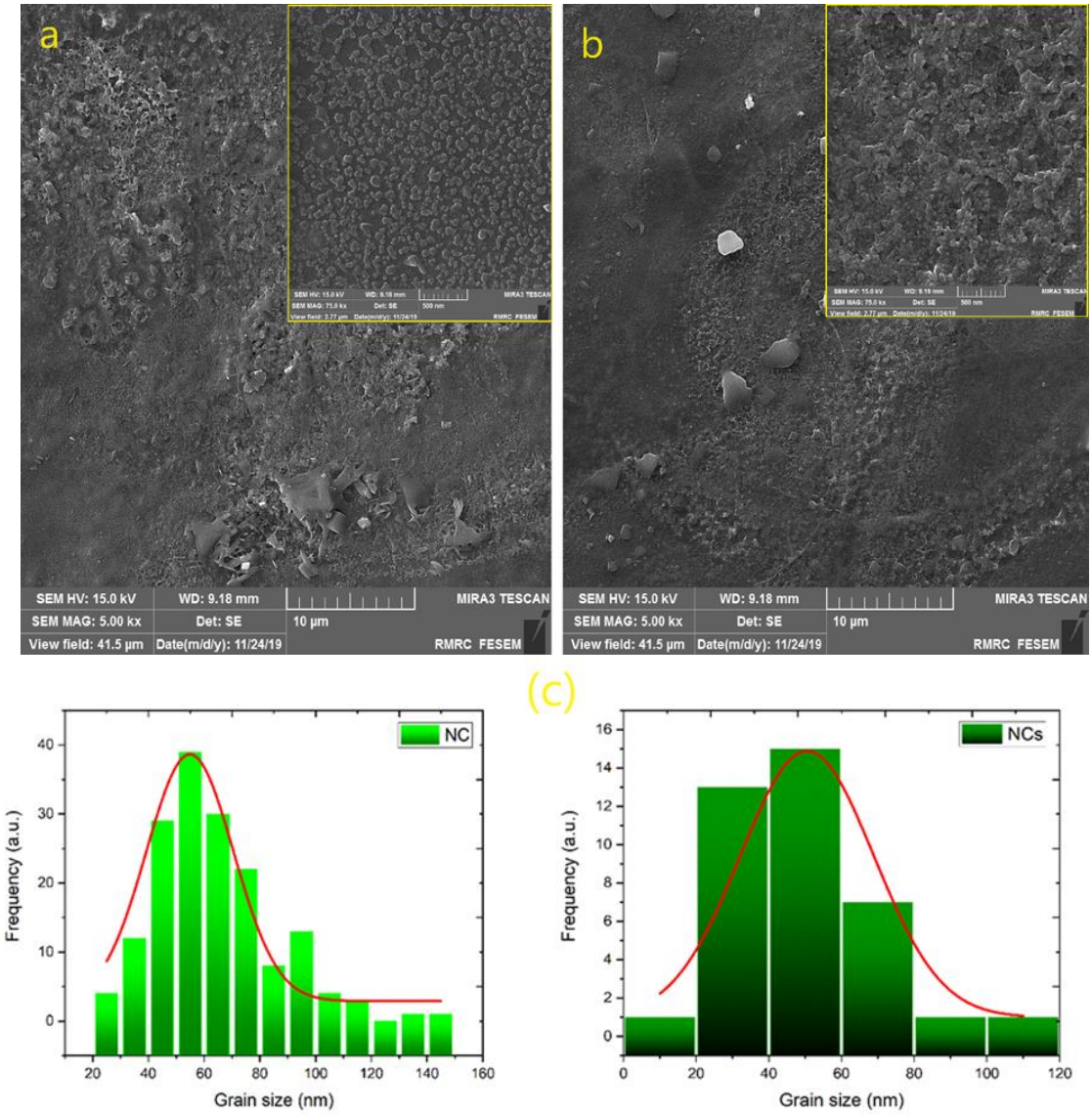

Fig. 4. FESEM images and grain size distribution of both NC and NCs thin films.

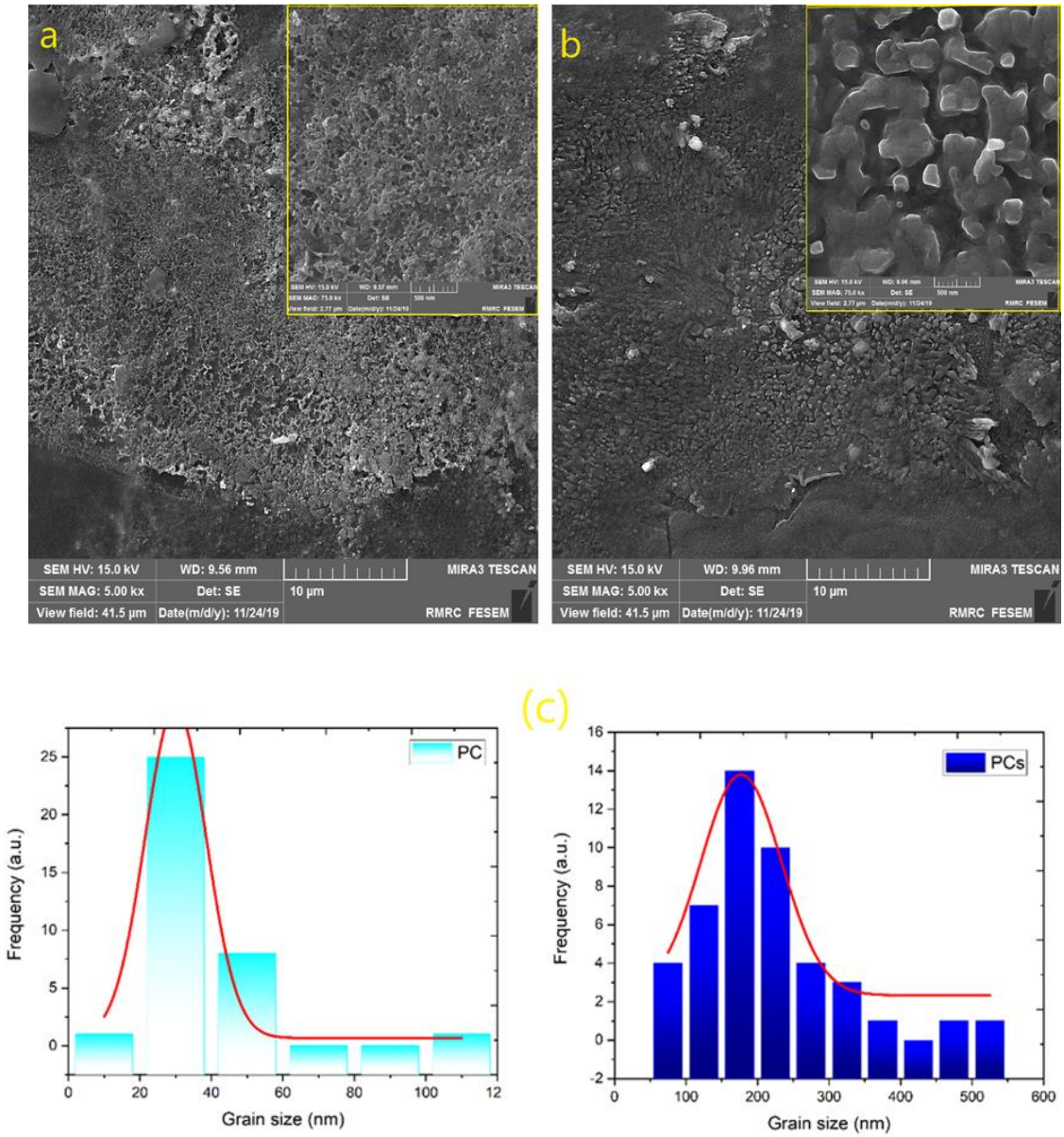

Fig. 5. FESEM images and grain size distribution of both PC and PCs thin films

3.3. Optical studies

Fig. 6 shows the optical transmission spectra of Cu_2ZnSnS_4 thin films with varying molar ratios of Zn/Sn. In the shorter wavelength region, the transmission of all samples increases with wavelength. The PV thin film exhibits higher transmittance in the 400-900 nm range compared to other PV thin films. After annealing, the NC thin film shows increased transmittance in the 400-1100 nm range, indicating improved surface structure. The PC thin film initially has a maximum transmittance of 60%, which decreases to 40% after annealing, particularly in shorter wavelengths. These findings, along with morphological and EDS results, provide insights into the optical and surface properties of the films, aligning with band gap calculations.

The optical band gap energy (E_g) of a film can be determined by plotting $(\alpha h\nu)^2$ against photon energy ($h\nu$) and identifying a linear region in the high-energy zone where α is close to zero. In this plot, (α) represents the absorption coefficient, ($h\nu$) represents the photon energy, and (A) is a constant. The equation used for this plot is:

$$(\alpha h\upsilon)^2 = A\,(h\upsilon - E_g) \quad (2)$$

By analyzing the linear portion of the plot, the value of the optical band gap energy (E_g) can be determined.

Fig. 7 illustrates the band gap energy of the samples. It was observed that the band gap energy increased in all samples after sulfurization, ranging from 1.50 eV to 1.66 eV. This increase in band gap energy can be attributed to several factors, including improvements in the structural and morphological properties of the material and changes in the elemental composition. After the annealing process, there is a reduction in the amount of sulfur in the sample compared to before annealing. This reduction in sulfur content leads to optical changes in the sample, causing the absorption edge to shift towards shorter wavelengths. As a

result, the band gap energy of the material increases, indicating a higher energy required for electronic transitions.

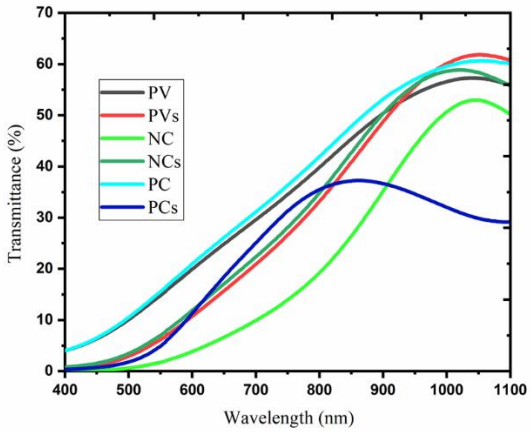

Fig. 6. The transmittance curves of CZTS thin films as a function of wavelength.

3.4. Electrical studies

To evaluate the electrical properties of the thin films, Hall effect and hot probe measurements were performed at room temperature. It was determined that all the samples exhibited p-type behavior. As shown in Table 3, the sulfurization process resulted in a decrease in sheet resistance (Rs) and resistivity (ρ) in the investigated thin films, while the carrier mobility (except for the PVs sample) and carrier density increased. Several factors can contribute to the reduction in sheet resistance. The enhancement in the crystalline and morphological structures of the thin films after annealing may have contributed to a decrease in carrier scattering, thereby leading to a decrease in sheet resistance. In the case of polycrystalline thin film semiconductors, an enlargement of the nanolayer dimensions can potentially enhance carrier mobility [26].

Table 3. Electrical measurement results of the CZTS thin films.

Sample	R_s ($\times 10^3$ Ω/square)	ρ (Ω.cm)	μ ($cm^2/V.S$)	p_{av} (cm^{-3})
PV	337.7	10.13	12.68	4.86×10^{16}
PVs	41.16	2.06	10.41	2.91×10^{17}
NC	514.29	15.43	9.27	4.37×10^{16}
NCs	28.62	1.43	12.18	3.58×10^{17}
PC	220.53	6.62	15.26	6.19×10^{16}
PCs	44.03	2.2	15.62	1.81×10^{17}

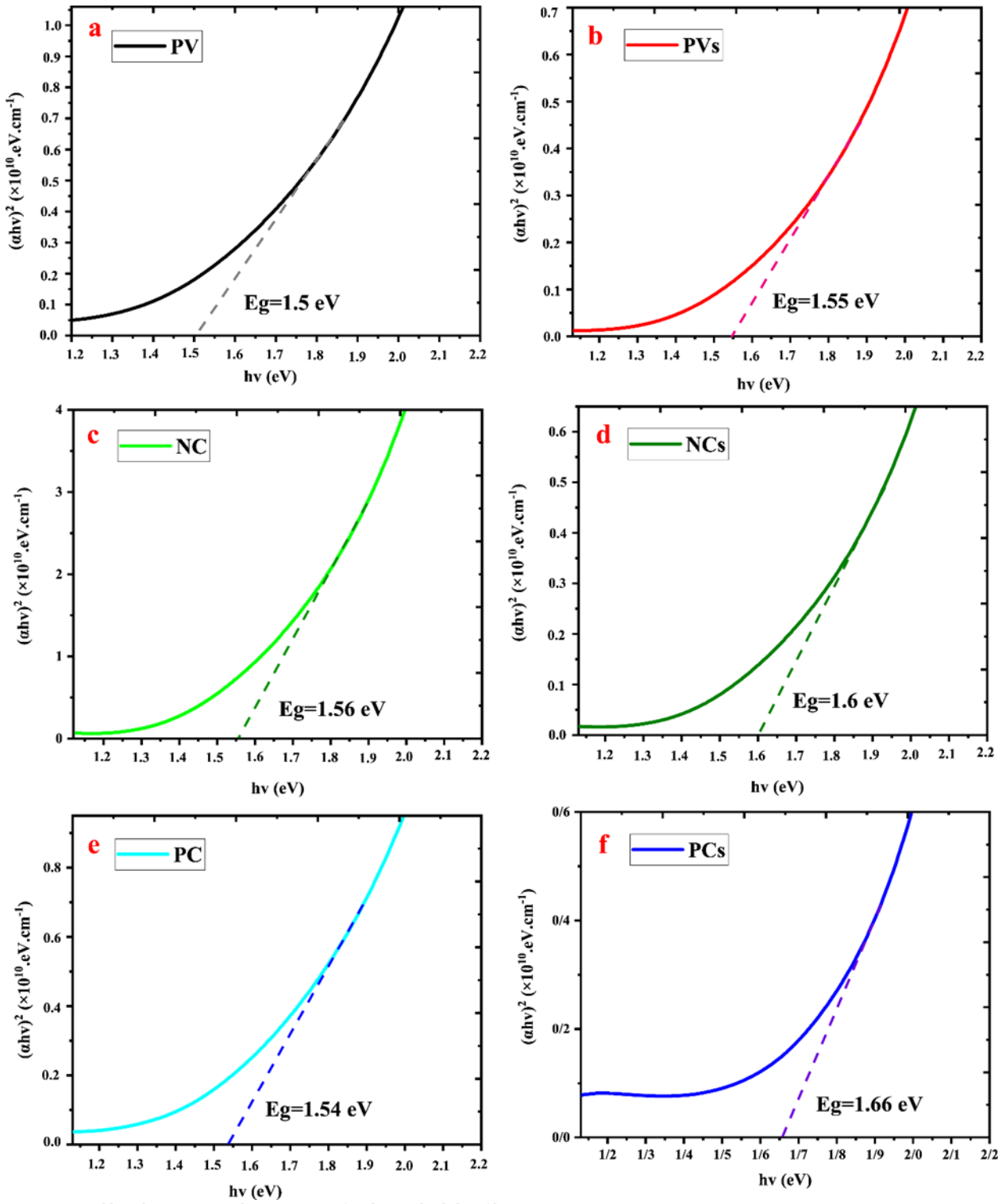

Fig. 7. Optical band gap versus photon energy for the studied thin films.

4. Conclusion

Cu_2ZnSnS_4 thin films were deposited on preheated glass substrates using the spray pyrolysis method at 325°C, with varying molar ratios of Zn and Sn. XRD analysis revealed that all the samples had a tetragonal structure with preferred orientation along the (112) plane, indicating a polycrystalline nature. After annealing, the band gap energy of all the samples increased, approaching the optimal value for absorber materials in thin-film solar cells. Hall effect and hot probe measurements showed that all the samples exhibited p-type conductivity. The NCs sample (Zn/ Sn= 0.29, Cu/ (Zn+ Sn) = 0.93, S/ (Cu+ Zn+ Sn) = 0.98) had the highest carrier density of 3.585×10^{17} cm^{-3} and the lowest specific resistivity of 1.43 Ω.cm. The highest carrier mobility was observed in the PCs sample (Zn/Sn = 2.84, Cu/ (Zn+ Sn) = 0.32, S/ (Cu+ Zn+ Sn) = 1.7). Overall, the spray pyrolysis method proved to be an effective approach for depositing Cu_2ZnSnS_4 thin films with desirable structural, optical, and electrical properties for photovoltaic applications.

Acknowledgements

There is nothing to acknowledgement.

Conflicts of Interest

The author declares that there is no conflict of interest regarding the publication of this article.

References

[1] Khemiri, N., Chamekh, S. and Kanzari, M., 2020. Properties of thermally evaporated CZTS thin films and numerical simulation of earth abundant and non toxic CZTS/Zn (S, O) based solar cells. *Solar Energy*, *207*, pp.496-502.

[2] Isotta, E., Syafiq, U., Ataollahi, N., Chiappini, A., Malerba, C., Luong, S., Trifiletti, V., Fenwick, O., Pugno, N.M. and Scardi, P., 2021. Thermoelectric properties of CZTS thin films: Effect of Cu–Zn disorder. *Physical Chemistry Chemical Physics*, *23*(23), pp.13148-13158.

[3] Tanaka, K., Oonuki, M., Moritake, N. and Uchiki, H., 2009. Cu2ZnSnS4 thin film solar cells prepared by non-vacuum processing. *Solar Energy Materials and Solar Cells*, *93*(5), pp.583-587.

[4] Xu, B., Qin, X., Lin, J., Chen, J., Tong, H., Qi, R., Yue, F., Chen, Y., Yang, P., Chu, J. and Sun, L., 2022. Positive role of inhibiting CZTSSe decomposition on intrinsic defects and interface recombination of 12.03% efficient kesterite solar cells. *Solar RRL*, *6*(8), p.2200256.

[5] Islam, M.F., Yatim, N.M. and Hashim, M.A., 2021. A review of CZTS thin film solar cell technology. *Journal of Advanced Research in Fluid Mechanics and Thermal Sciences*, *81*(1), pp.73-87.

[6] Sayed, M.H., Schoneberg, J., Parisi, J. and Guetay, L., 2018. Influence of silver incorporation on CZTSSe solar cells grown by spray pyrolysis. *Materials Science in Semiconductor Processing*, *76*, pp.31-36.

[7] Shockley, W. and Queisser, H., 2018. Detailed balance limit of efficiency of p–n junction solar cells. In *Renewable Energy* (pp. Vol2_35-Vol2_54). Routledge.

[8] Tanaka, K., Oonuki, M., Moritake, N. and Uchiki, H., 2009. Cu2ZnSnS4 thin film solar cells prepared by non-vacuum processing. *Solar Energy Materials and Solar Cells*, *93*(5), pp.583-587.

[9] Deokate, R.J., Chavan, H.S., Im, H. and Inamdar, A.I., 2022. Spray-deposited kesterite Cu2ZnSnS4 (CZTS): Optical, structural, and electrical investigations for solar cell applications. *Ceramics International*, *48*(1), pp.795-802.

[10] Wibowo, R.A., 2018. Powder-to-film approach for fabricating critical raw material-free kesterite Cu2ZnSn (S, Se) 4 thin film photovoltaic: A review. *Solar Energy*, *176*, pp.157-169.

[11] Wright, L.D., Lowe, J.C., Bliss, M., Tsai, V., Togay, M., Betts, T.R., Walls, J.M., Malkov, A.V. and Bowers, J.W., 2019. Water based spray pyrolysis of metal-oxide solutions for Cu2ZnSn (S, Se) 4 solar cells using low toxicity amine/thiol complexants. *Thin Solid Films*, *669*, pp.588-594.

[12] Bruc, L.I., Guc, M., Rusu, M., Sherban, D.A., Simashkevich, A.V., Shorr, S., Izquierdo-Roca, V., Pérez-Rodríguez, A. and Arushanov, E.K., 2012. Kesterite thin films of Cu2ZnSnS4 obtained by spray pyrolysis. In *Proceedings of 27th European Photovoltaic Solar Energy Conference and Exhibition* (pp. 2763-2766).

[13] Wang, K., Gunawan, O., Todorov, T., Shin, B., Chey, S.J., Bojarczuk, N.A., Mitzi, D. and Guha, S., 2010. Thermally evaporated Cu2ZnSnS4 solar cells. *Applied Physics Letters*, *97*(14).

[14] Xie, M., Zhuang, D., Zhao, M., Zhuang, Z., Ouyang, L., Li, X. and Song, J., 2013. Preparation and characterization of Cu 2 ZnSnS 4 thin films and solar cells fabricated from quaternary Cu-Zn-Sn-S target. *International Journal of Photoenergy*, *2013*.

[15] Singh, O.P., Muhunthan, N., Singh, V.N., Samanta, K. and Dilawar, N., 2014. Effect of temperature on thermal expansion and anharmonicity in Cu2ZnSnS4 thin films grown by co-sputtering and sulfurization. *Materials Chemistry and Physics*, *146*(3), pp.452-455.

[16] Yeh, M.Y., Lee, C.C. and Wuu, D.S., 2009. Influences of synthesizing temperatures on the properties of Cu 2 ZnSnS 4 prepared by sol–gel spin-coated deposition. *Journal of sol-gel science and technology*, *52*, pp.65-68.

[17] Kumar, S., Singh, P.K. and Chilana, G.S., 2009. Study of silicon solar cell at different intensities of illumination and wavelengths using impedance spectroscopy. *Solar Energy Materials and Solar Cells*, *93*(10), pp.1881-1884.

[18] Kumar, Y.K., Bhaskar, P.U., Babu, G.S. and Raja, V.S., 2010. Effect of copper salt and thiourea concentrations on the formation of Cu2ZnSnS4 thin films by spray pyrolysis. *physica status solidi (a)*, *207*(1), pp.149-156.

[19] Nakayama, N. and Ito, K., 1996. Sprayed films of stannite Cu2ZnSnS4. *Applied Surface Science*, *92*, pp.171-175.

[20] Kumar, Y.K., Babu, G.S., Bhaskar, P.U. and Raja, V.S., 2009. Preparation and characterization of spray-deposited Cu2ZnSnS4 thin films. *Solar Energy Materials and Solar Cells*, *93*(8), pp.1230-1237.

[21] Kameyama, T., Osaki, T., Okazaki, K.I., Shibayama, T., Kudo, A., Kuwabata, S. and Torimoto, T., 2010. Preparation and photoelectrochemical properties of densely immobilized Cu 2 ZnSnS 4 nanoparticle films. *Journal of Materials Chemistry*, *20*(25), pp.5319-5324.

[22] Stanchik, A.V., Gremenok, V.F., Juskenas, R., Tyukhov, I.I., Tivanov, M.S., Fettkenhauer, C., Shvartsman, V.V., Giraitis, R., Hagemann, U. and Lupascu, D.C., 2019. Effects of selenization time and temperature on the growth of Cu2ZnSnSe4 thin films on a metal substrate for flexible solar cells. *Solar Energy*, *178*, pp.142-149.

[23] Park, H., Hwang, Y.H. and Bae, B.S., 2013. Sol–gel processed Cu 2 ZnSnS 4 thin films for a photovoltaic absorber layer without sulfurization. *Journal of sol-gel science and technology*, *65*, pp.23-27.

[24] Ko, B.S., Kim, J.S., Jeon, D.H., Kang, J.K. and Hwang, D.K., 2018. Effects of back annealing on the structural and electrical properties of Cu2ZnSnSe4 thin films grown by a modified two-step process. *Science of Advanced Materials*, *10*(4), pp.580-585.

[25] Benaicha, M., Hamla, M. and Derbal, S., 2016. Electrochemical formation and selenization of ternary CuZnSn alloys for growing Cu2ZnSnSe4 photoactive thin films. *International Journal of Electrochemical Science*, *11*(6), pp.4909-4921.

[26] Abusnina, M., Moutinho, H., Al-Jassim, M., DeHart, C. and Matin, M., 2014. Fabrication and characterization of CZTS thin films prepared by the sulfurization of RF-sputtered

stacked metal precursors. *Journal of electronic materials*, *43*, pp.3145-3154.